

Quantitative Absorption Spectroscopy of a Single Gold Nanorod

Otto L. Muskens,[†] Guillaume Bachelier, Natalia Del Fatti,* and Fabrice Vallée

Université Lyon 1, Centre National de la Recherche Scientifique (CNRS), Laboratoire de Spectrométrie Ionique et Moléculaire (LASIM), 43 bd du 11 novembre, 69622 Villeurbanne cedex, France

Arnaud Brioude, Xuchuan Jiang, and Marie-Paule Pileni

Université Paris 6, CNRS, LM2N, 4 Place Jussieu, 75252 Paris cedex 05, France

Received: February 13, 2008; Revised Manuscript Received: March 19, 2008

The spectrally- and polarization-resolved absorption cross-sections of a single gold nanorod have been investigated using the spatial modulation spectroscopy technique. The ensemble of its optical features, that is, longitudinal and transverse surface plasmon resonances and interband absorption, has been quantitatively characterized. The results are compared with numerical simulations using the discrete dipole approximation and the finite element method, yielding information on the investigated nanorod size and shape.

Reduction of the size of a metal particle down to a nanometric scale is accompanied by large modifications of its optical properties, with apparition of new resonances. These features, the surface plasmon resonances (SPR), and the possibility of adjusting them by modifying the size, shape, structure, and environment of the nanoparticles are at the origin of the interest they have attracted during the past decade. Among the different synthesized nanoobjects, nanorods are of special interest because of the large amplitude and the tunability of their SPR, whose spectral position can be adjusted from the visible to the near-infrared by adapting their aspect ratio.¹ This opens up many possibilities for applications such as enhanced Raman scattering,² sensing or imaging,³ or local heating for medical applications.^{4,5} Furthermore, the large sensitivity of the SPR characteristics on the nanorod shape makes it an efficient tool for monitoring the rod-growing mechanism itself.⁶ Actually, slight modifications of the fabrication procedure can lead to large changes of the nanorod morphology and size.⁷ Key structural parameters, such as aspect ratio, cap-end shape, and volume of the particles, are frequently polydispersed, resulting in a strongly inhomogeneous optical response. This dispersion is preventing not only precise comparison of the experimental and computed spectra but also quantitative analysis of nanorod efficiency in applications such as those based on field enhancement effect. This limitation can be overcome by investigating a single nanorod. Scattering-based techniques have yielded precise spectral information on the main SPR of a nanorod, that is, corresponding to light polarized along its long axis.^{6,8,9} However, full analysis of the optical response of a single gold nanorod, including quantitative investigation of its transverse SPR and interband absorption cross-sections, has not yet been performed. Furthermore, quantitative measurements yield important information for most applications, providing insight in the amount of absorbed light energy per nanorod or the amplitude of the field enhancement effect, for instance. Actually, for the usually investigated sizes (nanorod diameter in the 15–20 nm range), the optical response, especially around the transverse SPR, is

dominated by absorption, making difficult a full characterization in scattering experiments.

Absorption-based methods for optical detection and spectroscopy of single metal nanoparticles have been recently demonstrated, thereby enabling, in particular, quantitative determination of the extinction cross-section of a nanoobject down to a few nanometers.^{10,11} This opens up the possibility of detailed determination of the optical response of a single nano-object over a large spectral range. Using the spatial modulation spectroscopy (SMS) technique,^{10,11} we have performed the first quantitative absorption spectroscopy of a single gold nanorod. Light-polarization dependent measurements allow us to identify the origin of the absorption features and to identify longitudinal and transverse SPR and interband absorption. The measured spectrally resolved extinction cross-sections have been quantitatively compared to numerical calculations based on the discrete dipole approximation (DDA) and finite element method (FEM), yielding information on the volume, aspect ratio, and shape of the investigated nanorod.

The gold nanorods are synthesized using a revisited procedure of that described in ref 2.^{7,13} Briefly, Au seeds are produced by mixing 1.25 mL of 0.002 M aqueous HAuCl₄ solution and 2.74 mL of 18 MΩ water in a test tube and then adding 3.76 mL of 0.20 M aqueous cetyl trimethylammonium bromide (CTAB) solution with further mixing. Finally, 0.9 mL of an aqueous 0.01 M NaBH₄ solution at 0 °C is added to the mixture, followed by vigorously shaking the solution. The growth solution (total volume of 8 mL) contains HAuCl₄·3H₂O (4.0 × 10⁻⁴ M), CTAB (0.095 M), and Ag⁺ (6.0 × 10⁻⁵ M), and the molar ratio of reducing agent (6.4 × 10⁻⁴ M) to [AuCl₄⁻] is kept at 1.6:1; they are added in a test tube one by one in that order. In the final step, the 2 h aged seed solution is added into the growth solution, and the final seed concentration [Au] seed is 5.0 × 10⁻⁷ M. The mixed solution is vigorously stirred for 20 s and then left undisturbed overnight.

The synthesized gold nanoparticles were characterized by transmission electron microscopy (TEM). A large majority of nanorods were observed, with only few particles with other shapes, mostly nanocubes (inset of Figure 1). Their length (*L*) is in the 40–60 nm range with a width (*D*) between 15 and 20 nm, corresponding to aspect ratios (*η*) ranging from 2 to 4. As

* Corresponding author e-mail: delfatti@lasim.univ-lyon1.fr.

[†] Present address: FOM-Institute AMOLF, Kruislaan 407, 1098SJ, Amsterdam, The Netherlands.

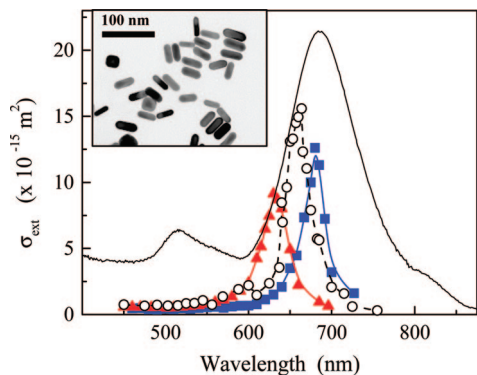


Figure 1. Absolute cross sections spectra measured for three different single gold nanorods, for a light polarization direction maximizing the amplitude of their main resonance (triangles, dots, and squares). The full line is the ensemble spectrum of the colloidal solution on an arbitrary scale. The inset shows a TEM image of the nanorods.

expected for nanorods, the ensemble absorption spectrum of the aqueous solution (Figure 1) exhibits two main resonances. The red-shifted peak at 680 nm corresponds to the longitudinal surface plasmon resonance. It is associated to the dipolar response of each nanorod polarized along its long axis (i.e., to electron oscillation along this direction induced by the incoming electromagnetic field). Its peak wavelength is known to strongly depend on the nanorod aspect ratio (η).^{14–16} The spectral position of the second resonance at 515 nm is consistent with the estimated wavelength of the transverse SPR of an ellipsoid (i.e., its dipolar response polarized along its short axis). In addition to transverse SPR of the nanorods, the resonance at 515 nm also contains contributions from other nanoparticles present in the solution.

The extinction spectra of individual gold nanorods are measured using the spatial modulation technique.^{10,11} This method is based on modulating, at a frequency (f) in the kHz range, the position of the studied nanoparticle in the focal plane of a tightly focused light beam. For this purpose, we use a transmission microscope consisting of two 100 \times , N.A. = 0.8 microscope objectives. The transmitted intensity is detected by a Si-photodiode and demodulated at the fundamental (f) or harmonic ($2f$) of the modulation frequency using a lock-in amplifier. The demodulated signal amplitude gives direct access to the nanoparticle extinction cross-section (σ_{ext}).¹¹ Because of the limited spatial resolution of this far-field technique, dilute samples have to be prepared (with a surface density of typically less than one particle per square micrometer). This is done by spincoating onto a glass substrate a drop of the gold nanorod solution after addition of a polymer (PVOH). Nanoparticles embedded in a thin layer of polymer are thus obtained, providing them with a relatively homogeneous environment. The sample is mounted on the piezoelectric shaker, and the ensemble is displaced in the focal plane by a X - Y piezo-stage for two-dimensional (2D) imaging of the sample surface. For σ_{ext} spectrum measurements, this system is associated to a broadly tunable source.¹¹ This is based on supercontinuum generation in a photonic crystal fiber injected by a femtosecond pulse train delivered by a homemade 20 fs Ti/sapphire oscillator working at 780 nm. A spectral bandwidth of about 3 nm is filtered out of the generated unpolarized white-light continuum using a grating pair system. After selection of a linear polarization direction, it is used as the light source for the spatial modulation microscope. In these studies, both absorption and scattering contribute to the measured extinction cross-section. However, for a small particle the latter yield a small contribution, and

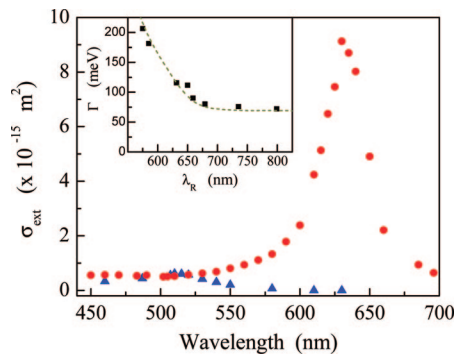


Figure 2. Absolute extinction cross-section of a single gold nanorod measured using the SMS technique. The two spectra (dots and triangles) have been obtained for two orthogonal linear polarizations ($\alpha = 87^\circ$ and 177°). Inset: Full width half-maximum (fwhm) of the main resonance as a function of its wavelength measured in different single nanorods. The dotted line is the computed width using eq 2 with the dielectric function of gold reported by Johnson and Christy.¹⁷

absorption dominates the observed extinction. This is the case for the single nanorods investigated here (see below).

Polarized extinction spectra measured for different single gold nanorods are shown in Figure 1. For these spectra, the polarization of the incident light was rotated to maximize the amplitude of extinction in the 600–700 nm range. The shape and strong dependence of the resonances on the linear polarization of the incident light is characteristic of a nanorod-like object. Most of the investigated nanoparticles show this spectral signature, with only few particles exhibiting different wavelength and polarization responses. These deviating spectra have been attributed to the presence of nano-objects with different shapes, in agreement with TEM measurements (Figure 1, inset), and will not be discussed here.

The extinction around the long wavelength resonance at about 630 nm is strongly polarization dependent (Figure 2). This is better shown by plotting the measured extinction cross section as a function of the polarization direction (α) of the incident light defined in the laboratory frame (Figure 3). As expected for the longitudinal surface plasmon resonance of a small nanorod, a purely dipolar behavior is observed with a very high polarization contrast ratio exceeding 10^2 (ratio between the maximum and minimum extinction cross sections, Figure 3a). This polarization dependence is lost by orientational averaging in ensemble measurements. In single particle experiments, the maximum amplitude corresponds to the nanorod long axis whose orientation on the substrate can thus be precisely determined. Defining it by the angle α_L relative to the laboratory frame and fitting the data using eq 1,

$$\sigma_{\text{ext}}(\alpha; \lambda) = \sigma_{\parallel}(\lambda) \cos^2(\alpha - \alpha_L) + \sigma_{\perp}(\lambda) \sin^2(\alpha - \alpha_L) \quad (1)$$

$\alpha_L = 87 \pm 1^\circ$ is obtained for the nanorod displayed in Figure 2. The extinction cross-section at the longitudinal SPR wavelength is precisely determined; $\sigma_{\text{ext}}(\alpha_L) = \sigma_{\parallel} = 9.2 \times 10^3 \text{ nm}^2$ (with $\sigma_{\perp} \approx 0$). Note that σ_{ext} can be crudely estimated from the ensemble spectrum by assuming that all the gold ions are reduced and using the nanorod mean size. The obtained value of $2.5 \times 10^3 \text{ nm}^2$ at the mean SPR wavelength is of the same order of magnitude but is considerably smaller than the one measured for individual nanorods, because of the SPR inhomogeneous broadening.

Actually, spectra recorded for different single nanorods show a large dispersion of the SPR wavelength (Figure 2 inset), ascribed to fluctuations in the nanoparticle aspect ratio and/or

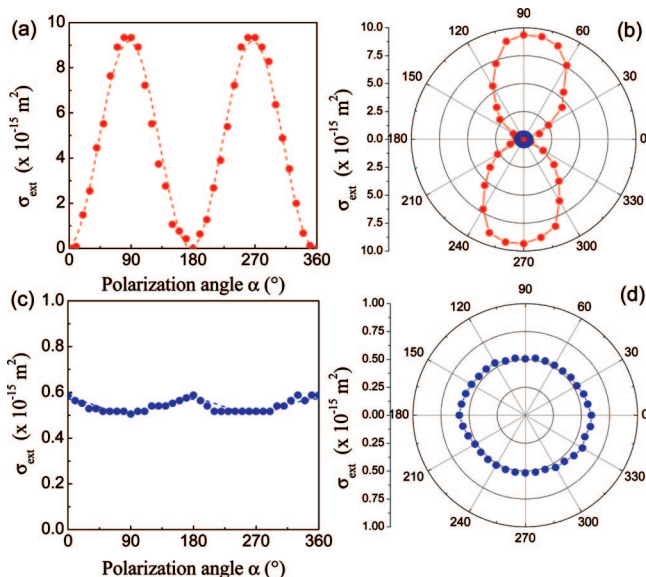


Figure 3. Linear and polar plot of the polarization dependence of the extinction cross section measured for the gold nanorod of Figure 2 at the longitudinal (panels a and b, $\lambda \approx 630$ nm) and transverse (panels c and d, $\lambda \approx 515$ nm) SPR (the latter data are also shown in panel b). The dashed lines in panels a and b are fit of the experimental data using eq 1, with $\alpha_L = 87^\circ$, $\sigma_{||}(630 \text{ nm}) = 9.2 \times 10^3 \text{ nm}^2$, and $\sigma_{\perp}(630 \text{ nm}) = 0$; $\sigma_{||}(515 \text{ nm}) = 510 \text{ nm}^2$ and $\sigma_{\perp}(515 \text{ nm}) = 570 \text{ nm}^2$.

environment. This translates into a large inhomogeneous broadening of the SPR feature measured in ensemble, which exhibits a much larger width than for a single nanorod (Figure 2). For the latter, the measured full width half-maximum (fwhm) Γ corresponds to the intrinsic one due to SPR damping. Its increase with decreasing the SPR wavelength λ_{ext} and its absolute value are consistent but slightly smaller than previous dark-field scattering measurements (about 75 meV as compared to 80 meV for $\lambda_{\text{ext}} \approx 730$ nm).^{8,9} As a first approximation, the theoretical longitudinal SPR width can be estimated from the extinction cross-section of a spheroid in the quasistatic approximation, which has the advantage of taking a simple analytic form.¹⁸ A quasi-Lorentzian profile for the SPR is obtained if the imaginary part (ϵ_2) and interband contribution to the real part of the metal dielectric function are weakly dispersed around the SPR frequency (ω_R).^{19,20} Its width (Γ) can then be properly defined and takes the same form as in a nanosphere under the same approximations,

$$\Gamma = \frac{\omega_R^3}{\omega_p^2} \epsilon_2(\omega_R) \approx \gamma + \frac{\omega_R^3}{\omega_p^2} \epsilon_2^{\text{ib}}(\omega_R) \quad (2)$$

where ω_p is the plasma frequency, γ is the mean conduction electron scattering rate, and ϵ_2^{ib} is the interband contribution to ϵ_2 . These approximations are valid when the SPR is away from the metal interband transitions, as in the case of gold nanorods or silver nanospheres.^{19,20} For scattering cross-sections, the same width is computed, under the same approximations. The measured data are in excellent agreement with the estimated Γ , using the bulk ϵ_2 values reported by Johnson and Christy,¹⁷ without introducing additional broadening effects such as electron–surface scattering or radiative damping. This confirms that they play minor roles and that Γ is dominated by bulk-like electron interaction effects for the investigated sizes.⁹ In the long wavelength range, Γ is set by the electron scattering rate (γ) and is thus almost constant. In the short wavelength range, ϵ_2^{ib} increases, reflecting the rise of the interband absorption. SPR

damping due to interband electron excitation becomes significant, leading to the observed increase of Γ (Figure 2, inset).⁸ Our data are also consistent with the values of Γ reported by Palik,²¹ with the main difference being the prediction of a larger long wavelength Γ value: about 85 meV instead of 69 meV, the experimental value being 72 meV (detailed comparison is, however, difficult because of the large energy step of the ϵ data in the wavelength range of interest).

In the small wavelength range, below 550 nm, a weak resonance is observed around 510 nm for light polarization perpendicular to that maximizing the 630 nm SPR. This is better observed by plotting the measured extinction cross-section as a function of the light polarization direction. A maximum amplitude is observed for light polarization directions $\alpha_T \approx 357$ or 177° with, conversely to the long wavelength resonance, only a weak contrast of about 1.1 (Figure 3). In this spectral range, absorption is dominated by the polarization independent interband transitions in gold. The observed weak polarization effect is ascribed to enhancement of this absorption by the transverse surface plasmon resonance that is observed for the first time on a single nanoparticle here. Its amplitude is strongly reduced by its large broadening, a consequence of its overlap with the interband transitions.

The large sensitivity of the optical response of a nanorod on its geometry (volume, aspect ratio, and tip shape) reflects in the uncorrelated rod-to-rod variation of its SPR wavelength and amplitude (Figure 1). In particular, for an ellipsoid of fixed volume, σ_{ext} is expected to increase with λ_R ,²² in contrast to the experimental observation (Figure 1), probably because of volume fluctuations. This is an important parameter for application, absorption, or field enhancement effects strongly depending not only on the nanoparticle aspect ratio but also on its full size. It can be addressed here since the absolute σ_{ext} value is determined. To more precisely analyze the impact of the nanorod shape and size, we have quantitatively compared our experimental data with that of numerical modeling. Discrete dipole approximation (DDA) or finite element method (FEM) were used, both approaches permitting description of an arbitrary shape nano-object.^{23–26}

In the DDA method the studied nano-object is represented as a cubic lattice of N polarizable point dipoles subject to a monochromatic plane wave.²³ The obtained complex linear equations were solved with the code adapted by Draine and Flatau.²⁷ An important parameter is the number of dipoles mimicking the homogeneous particle to converge the computed physical quantities.²⁸ As cross-sections are accurate to a few percent for typically $N \approx 10^4$ dipoles, about 4×10^4 dipoles were used here. FEM simulations were performed with the COMSOL Multiphysics software. The electric field around the nanorod was computed using both the weak form and the scattered field formulation.²⁶ To avoid spurious reflection effects at the simulation zone boundaries, perfectly matched layers (PML) were used as an anisotropic absorber coating the matrix in which the nanorod is embedded.²⁶ Absorption and scattering cross-sections were computed by integrating the absorbed power over the nanorod volume and the Poynting vector flux over the matrix boundary, respectively. Both mesh and PML parameters were optimized to give excellent agreement with the Mie theory for spherical particles.

In both calculations, the gold nanoparticles were described using the bulk dielectric function (ϵ) measured by Johnson and Christy,¹⁷ as they yield the best agreement with the measured longitudinal SPR width (Figure 2). Furthermore, using the ϵ data reported by Palik leads to additional structures that only

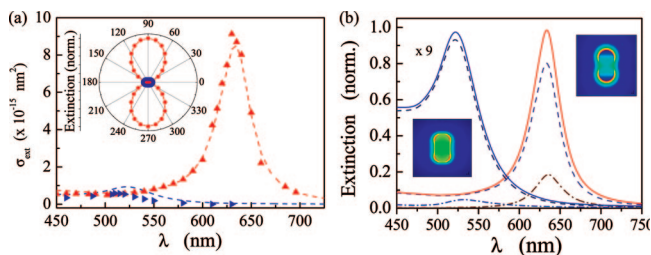


Figure 4. (a) Computed (dashed lines) and measured (triangles) absolute values of the extinction cross section of a single nanorod for two linear polarizations parallel or perpendicular to the main rod axis. A cigar-like shape with an aspect ratio of $\eta \approx 2$ is assumed in the calculation. Inset: polar plot of the computed extinction polarization dependence close to the longitudinal $\lambda = 640$ nm (red dots) and transverse $\lambda = 525$ nm (blue thick line) SPRs. (b) Computed absorption (dashed lines) and scattering (dash-dotted lines) contributions to the optical extinction (full lines) for light polarized perpendicular (blue-shifted resonance, with amplitude multiplied by 9) or along (red-shifted resonance) the main rod axis. The images show the electric field amplitude around the particle for light polarized along the long (short) axis at 640 (525) nm.

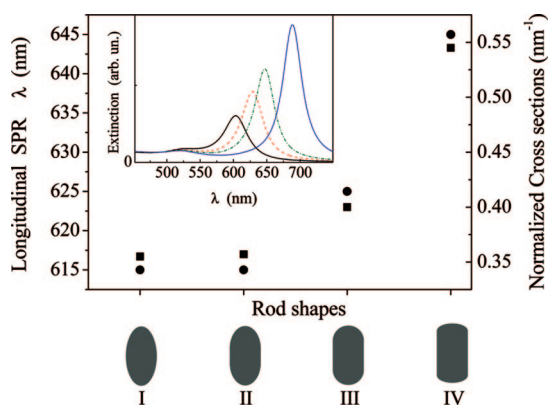


Figure 5. Longitudinal surface plasmon resonance wavelength (dots) and peak extinction cross section per unit nanorod volume (squares) computed for four different gold nanorod shapes. They all correspond to a total rod length of 30 nm and a diameter of 15 nm ($\eta = 2$). Inset: calculated dependence of the extinction spectrum on the nanorod aspect ratio $\eta = 1.75$ (solid, black), 2 (dashed, red), 2.15 (dash-dotted, green), and 2.5 (solid, blue), for a cigar-like shape (III).

reflect the unsmoothness of the measured ϵ_1 in this range.²⁹ These new resonances, predicted in the 500–600 nm wavelength range (particularly visible for small aspect ratio nanorods \square), are neither observed experimentally nor obtained by using the Johnson and Christy data. Following previous results performed in similar conditions for nanospheres,¹⁰ the dielectric constant of the polymer environment was assumed to be homogeneous with $\epsilon_m = 2.1$. Because the optical response depends on the nanoparticle shape, and to mimic the actual one observed with TEM (Figure 1), simulations were performed for cigar-like shaped particles formed by a cylinder of length l , diameter D , and capped by hemispheres of radius $D/2$ (Figure 4b and shape III in Figure 5). The remaining parameters in comparing the experimental and simulated extinction cross-sections (σ_{ext}) are thus only l and D , which translate into the particle volume (V) and aspect ratio, $\Gamma = 1 + l/D$. The former essentially sets the amplitude of σ_{ext} and is actually the only parameter in the interband transition region ($\lambda \leq 500$ nm). In contrast, as for a prolate ellipsoid, the latter determines the wavelength and amplitude of the SPRs with a much larger sensitivity for the longitudinal one (Figure 5, inset).

A good reproduction of the measured extinction spectra for different single nanorods is obtained with a cigar-like shape

(shape III in Figure 5) as illustrated in Figure 4. The DDA and FEM models yield similar results, with deviation of the computed peak wavelength of less than 5 nm. Both the amplitude and the shape of the polarization-dependent spectra are well-reproduced assuming $D = 25.5$ nm and a full length $L = l + D = 50$ nm (the incident light polarization is polarized either along the short or long axis of the rod, the latter being identified with the 90° direction). In both cases, as expected for relatively small rods, absorption strongly dominates over scattering, with the latter contributing less than 20% and 5% of the extinction at the longitudinal and transverse SPR wavelength, respectively (Figure 4b). For light polarized along the rod axis, excellent reproduction of the spectral position, width, and amplitude of the main resonance is obtained. In particular, the computed fwhm of about 115 meV is in excellent agreement with the estimated one using eq 2 (Figure 2, inset). Furthermore, as observed experimentally (Figure 3), a dipolar type of dependence of σ_{ext} on light polarization is computed at the longitudinal SPR wavelength with a much smaller variation than that of the transverse SPR (Figure 4). Actually, although the amplitude of the interband transition is also well-reproduced away from the SPR, the computed properties of the latter significantly differ from the experimental one; its calculated spectral position is slightly red-shifted and, concomitantly, its amplitude is larger (its broadening due to overlap with the interband transitions being reduced).

This discrepancy can probably be ascribed to the nanorod geometry chosen for the calculation. Although the used shape seems more realistic than the pure cylinder^{16,30} or the ellipsoidal model, it contains a degree of arbitrariness. Actually, the shape of the end caps has an important impact on the calculated position and amplitude of the SPR.^{31,32} This is illustrated in Figure 5, showing the red-shift and peak amplitude increase of the longitudinal SPR when flattening the nanorod caps, that is, evolving from a prolate ellipsoid (I) to a quacylinder (IV), keeping the same aspect ratio (the extinction cross-section is normalized to the nanorod volume to show only its shape dependence). This evolution is similar to that induced by an increase of the nanorod aspect ratio (inset of Figure 5 for a cigar-like rod). Actually, as the cap shape differently influence the longitudinal and transverse SPR, it constitutes an additional parameter to better reproduced the experimental data.^{31,32} Using the relative extinction cross-section of the two SPR as the relevant criterion, a very good reproduction of the data is obtained, sharpening the nanorod shape. However, although this shape modification yields excellent results, it might compensate for other effects such as slight nanorod asymmetry or local variation of the dielectric constant of the surrounding matrix. More detailed experimental–theoretical comparison requires limiting the number of involved parameters, for instance, by performing electron microscopy and optical measurements on the same nanoparticle.^{33,34}

In conclusion, the extinction spectra of single nanorods have been investigated using the spatial modulation technique. In contrast to previous scattering based studies of single nanorods,^{8,9} the measured signal yields access to the absorption of a single nanorod. This permits observation of both its longitudinal and transverse surface plasmon resonances. The additional information brought by determination of the absolute value of the extinction cross-section and measurement of the transverse SPR permit detailed comparison with theoretical models. Quantitative agreement with the results of DDA and FEM simulations is obtained by assuming a nanorod with a cigar-like shape. These results open up many possibilities for precise investigation of

detailed shape effects on the optical properties of metal nanoparticles and for their in situ characterization before nonlinear optical studies.³⁵ Such precise quantitative investigation is also a prerequisite for using single nanoparticle as a calibrated local absorber or local field enhancer.

Acknowledgment. The authors would like to thank Institut Universitaire de France (IUF).

References and Notes

- (1) Murphy, C. J.; Sau, T. K.; Gole, A. M.; Orendorff, C. J.; Gao, J.; Gou, L.; Hunyadi, S. E.; Li, T. *J. Phys. Chem. B* **2005**, *109*, 13857.
- (2) Nikoobakht, B.; Wang, Z.; El-Sayed, M. A. *Chem. Phys. Lett.* **2002**, *366*, 17.
- (3) Mohamed, M. B.; Volkov, V.; Link, S.; El-Sayed, M. A. *Chem. Phys. Lett.* **2000**, *317*, 51.
- (4) McFarland, A. D.; van Duyn, R. P. *Nano Lett.* **2003**, *3*, 1057.
- (5) (a) Huang, X.; El-Sayed, I. H.; Qian, W.; El-Sayed, M. A. *J. Am. Chem. Soc.* **2006**, *128*, 2115. (b) Huff, T. B.; Tong, L.; Zhao, Y.; Hansen, M. H.; Cheng, J.-X.; Wei, A. *Nanomedicine* **2007**, *2*, 125.
- (6) Boleininger, J.; Kurz, A.; Reuss, V.; Sönnichsen, C. *Phys. Chem. Chem. Phys.* **2006**, *8*, 3824.
- (7) Jiang, X. C.; Pileni, M. P. *Colloids Surf. A* **2007**, *295* (1–3), 228–232.
- (8) Sönnichsen, C.; Franzl, T.; Wilk, T.; von Plessen, G.; Feldmann, J.; Wilson, O.; Mulvaney, P. *Phys. Rev. Lett.* **2002**, *88*, 077402.
- (9) Novo, C.; Gomez, D.; Perez-Juste, J.; Zhang, Z.; Petrova, H.; Reismann, M.; Mulvaney, P.; Hartland, G. V. *Phys. Chem. Chem. Phys.* **2006**, *8*, 3540.
- (10) Arbouet, A.; Christofilos, D.; Del Fatti, N.; Vallée, F.; Huntzinger, J.-R.; Arnaud, L.; Billaud, P.; Broyer, M. *Phys. Rev. Lett.* **2004**, *93*, 127401.
- (11) Muskens, O.; Del Fatti, N.; Vallée, F.; Huntzinger, J.-R.; Billaud, P.; Broyer, M. *Appl. Phys. Lett.* **2006**, *88*, 063109.
- (12) Murphy, C. J.; Jana, N. R. *Adv. Mater.* **2002**, *14*, 80.
- (13) Jiang, X. C.; Brioude, A.; Pileni, M. P. *Colloids Surf. A* **2006**, *277*, 201.
- (14) El-Sayed, A.-M.; Majied, A.-S. *Colloids Surf. A* **2004**, *246*, 61.
- (15) Pérez-Juste, J.; Liz-Marzan, L. M.; Carnie, S.; Chan, D. Y. C.; Mulvaney, P. *Adv. Funct. Mater.* **2004**, *14*, 571.
- (16) Brioude, A.; Jiang, X. C.; Pileni, M. P. *J. Phys. Chem B* **2005**, *109*, 13138.
- (17) Johnson, P. B.; Christy, R. W. *Phys. Rev. B* **1972**, *6*, 4370.
- (18) Kreibig, U.; Vollmer, M.; , *Optical Properties of Metal Clusters*; Springer: Berlin, 1995.
- (19) Del Fatti, N.; Vallée, F.; Flytzanis, C.; Hamanaka, Y.; Nakamura, A. *Chem. Phys.* **2000**, *251*, 215.
- (20) Voisin, C.; Del Fatti, N.; Christofilos, D.; Vallée, F. *J. Phys. Chem. B* **2001**, *105*, 2264.
- (21) *Handbook of Optical Constants of Solids*, Palik, E.D., Ed.; Academic Press: New York, 1985.
- (22) Muskens, O.; Christofilos, D.; Del Fatti, N.; Vallée, F. *J. Opt. A* **2006**, *8*, 264.
- (23) Purcell, E. M.; Pennypacker, C. R. *Astrophys. J.* **1973**, *186*, 705.
- (24) Salzemann, C.; Lisiecki, I.; Brioude, A.; Urban, J.; Pileni, M. P. *J. Phys. Chem. B* **2004**, *108* (35), 13242–13248.
- (25) Kelly, K. L.; Coronado, E.; Zhao, L. L.; Schatz, G. C. *J. Phys. Chem. B* **2003**, *107*, 668.
- (26) Jin, J.; *The Finite Elements Method in Electrodynamics*; Wiley Interscience: New York, 2002.
- (27) Draine, B. T.; Flatau, P. J. *J. Opt. Soc. Am. A* **1994**, *11*, 1491.
- (28) Sosa, I. O.; Noguez, C.; Barrera, R. G. *J. Phys. Chem. B* **2003**, *107*, 6269.
- (29) Blanchard, N. P.; Smith, C.; Martin, D. S.; Hayton, D. J.; Jenkins, T. E.; Weightman, P. *Phys. Status Solidi C* **2003**, *8*, 2931.
- (30) Brioude, A.; Pileni, M. P. *J. Phys. Chem B* **2005**, *109*, 23371.
- (31) Prescott, S. W.; Mulvaney, P. *J. Appl. Phys.* **2006**, *99*, 123504.
- (32) Lee, K.-S.; El-Sayed, M. A. *J. Phys. Chem B* **2005**, *109*, 20331.
- (33) Hu, M.; Chen, J.; Marquez, M.; Xia, Y.; Hartland, G. V. *J. Phys. Chem. C* **2007**, *111*, 12558.
- (34) Billaud, P.; Marhaba, S.; Cottancin, E.; Arnaud, L.; Bachelier, G.; Bonnet, C.; Del Fatti, N.; Lermé, J.; Vallée, F.; Vialle, J.-L.; Broyer, M.; Pellarin, M. *J. Phys. Chem. C* **2008**, *112*, 978.
- (35) Muskens, O. L.; Del Fatti, N.; Vallée, F. *Nano Letters* **2006**, *6*, 552.

JP8012865